24th COBEM - 2017

24th ABCM International Congress of Mechanical Engineering
December 3-8, 2017, Curitiba, PR, Brazil

COBEM-2017-0232
PRESSURE RATIO INFLUENCE OVER THE PERFORMANCE OF A SCROLL EXPANDER

Fernando Vieira de Oliveira
fernandovo@yahoo.com.br

Filipi Martins Fernandes Silva
filipimfs@gmail.com

Paulo Eduardo Batista de Mello
Centro Universitário da FEI – Av. Humberto de Alencar Castelo Branco, 3972 - São Bernardo do Campo - São Paulo - Brazil
pmello@fei.edu.br

Abstract. *The use of scroll expanders in Organic Rankine Cycle (ORC) and Compressed Air Energy Storage (CAES) systems have been considered as a good alternative by many research studies presented in the last decades. These devices are appropriate for the low power range, usually between 1 and 10 kW. Small distributed generation sites could benefit from using scroll devices. One important finding from previous work is the fact that internal leakages decrease the isentropic efficiency of scroll expanders. Actually, these leakages are the main cause of inefficiency. In this paper, a transient 2D CFD simulation of a scroll expander capable of quantifying the internal leakages was used. The results obtained show that the leakages can influence the point of maximum isentropic efficiency of the device, related to pressure ratio. Normally, this maximum is closely related to expander volume ratio, but high internal leakages tend to reduce the optimum pressure ratio. The computation of other relevant parameters (filling factor and power) support the findings and explains the behavior of the measurements obtained with a scroll prototype.*

Keywords: *Scroll expander, CFD simulation, pressure ratio, internal leakage, ORC*

1. INTRODUCTION

Scroll expanders are appropriate for the construction Organic Rankine Cycle (ORC) of low power, with range between 1 and 10 kW, according to Quoilin et al. (2013). These devices may also be used as main component of Compressed Air Energy Storage (CAES) systems. These relevant applications of scroll expanders have attracted the attention of several researchers, particularly for waste heat recovery (WHR) systems.

The scroll device was invented in 1905 by Creux and was further developed for using in compressors and vacuum pumps. Its use as an expander device is recent, with the first proposals made 20 years ago, with first promising results obtained by Zanelli and Fravat (1994). In this study, the authors proposed two parameters to characterize the machine performance still in use nowadays: filling factor and isentropic efficiency.

Using one appropriate experimental setup, Yanagisawa et al. (2001) converted a commercial scroll compressor into an expander. This expander presented isentropic efficiency ranging from 60% to 65%, tested with air. In more recent research, Declaye et al. (2013) and Mendoza et al. (2014) reported 75.7% and 61%, respectively. The studies revealed that the scroll performance depends on the presence of oil mixed with the working fluid. Oil free expanders present higher internal leakages and, consequently, lower isentropic efficiency.

Lemort et al. (2009) proposed a model to predict the performance of a scroll expander, which has been intensively tested, presenting very good agreement with experiments. According to the authors, the main losses present in the device are: internal leakages (flank and radial leakages) and under-expansion or over-expansion. Other losses less relevant are the pressure drop at inlet, heat transfer and friction.

Simulations of scroll expanders using CFD (computational fluid dynamics) are more recent. Song et al. (2015a) listed nine relevant previous work on the last 27 years about numerical simulation of scrolls. The authors said these simulations are in an early stage, due the motion and the complex geometry of this device.

Wei et al. (2015) performed a 3D transient simulation investigating the suction process of scroll expander operating with R123, an organic fluid. An unstructured dynamic mesh technology was applied. Validating the numerical model, they tested its machine in an ORC bench for WHR. The mass flow, torque and pressure distributions were some of the

results. With this same methodology, Song et al. (2015b) obtained 55% output power deviation between experiment and simulation. According the authors, this difference is due the adiabatic simulation models that ignored all the mechanical transmission losses. In addition, the leakage flow losses in the axial clearances and the heat flow losses were not considered in this study.

Silva (2017) demonstrates that a 2D simulation of a scroll expander presents small differences when compared to a 3D simulation, but the second demands much higher resources and computational time.

The present work focusses on evaluating the pressure ratio influence over the scroll expander performance. The isentropic efficiency, filling factor and power are computed. These parameters are widely used in previous experimental work to characterize the performance of expanders. The results are compared with the experimental tests presented by Romão (2017). To maintain computational time as low as possible, only two dimensional simulations were performed.

2. GEOMETRY

The geometry of the scroll walls is defined by involute of a circle. This section presents the equations used to construct the scroll curves, discussed in detail by Blunier et al. (2009) who described the curves using radius of the involute basic circle r_b and angles φ that define the start and ending points of the different curves. The authors used an orthonormal frame, defined by a tangent vector Eq. (1) and by a unit normal vector Eq. (2).

$$\mathbf{t}(\varphi) = (\cos\varphi, \sin\varphi) \tag{1}$$

$$\mathbf{n}(\varphi) = (-\sin\varphi, \cos\varphi) \tag{2}$$

The external and internal walls of the fixed scroll are described by Eq. (3) and Eq. (4), respectively. The angles φ_{es} e φ_{is} are the external and internal starting angles, φ_{e0} and φ_{i0} the initial angles of the external and internal curves, $\varphi_{\max}$ the involute ending angle.

$$\mathbf{S}_{fe}(\varphi) = r_b\,\mathbf{t}(\varphi) - r_b(\varphi - \varphi_{e0})\mathbf{n}(\varphi) \qquad \forall\varphi \in I_e = \lfloor \varphi_{es}, \varphi_{\max} \rfloor \tag{3}$$

$$\mathbf{S}_{fi}(\varphi) = r_b\,\mathbf{t}(\varphi) - r_b(\varphi - \varphi_{i0})\mathbf{n}(\varphi) \qquad \forall\varphi \in I_i = [\varphi_{is}, \varphi_{\max}] \tag{4}$$

The orbiting scroll wall is described like the fixed one offsetted by π. The orbiting angle θ defines the relative position between fixed and moving scroll. The external and internal moving walls are described, respectively, by Eq. (5) and Eq. (6).

$$\mathbf{S}_{me}(\varphi) = -\mathbf{S}_{fe}(\varphi) - r_o\mathbf{n}(\theta) \tag{5}$$

$$\mathbf{S}_{mi}(\varphi) = -\mathbf{S}_{fi}(\varphi) - r_o\mathbf{n}(\theta) \tag{6}$$

Both scrolls have constant thickness, determined by Eq. (7).

$$e = r_b(\varphi_{i0} - \varphi_{e0}) \tag{7}$$

The use of the nominal orbiting radius r_o, defined by Eq. (8) would result in contact between the fixed and the orbiting scroll. Hence, to avoid it, the orbiting radius is reduced creating a gap between the walls and, consequently, a leakage path. The size of this gap should consider constructive aspects like the tolerances utilized to construct the machine. A gap as small as possible is desirable for less flank leakages increasing the efficiency of the device.

$$r_o = r_b(\varphi_{e0} - \varphi_{i0} + \pi) \tag{8}$$

The parameters that permit to construct the geometry of the scroll prototype used for validation (Fanti et al., 2016) are presented in Tab 1. As the nominal orbiting radius is 6.5 mm while the orbiting radius is 6.335 mm, a gap of 0.165 mm is created. This value of gap and parameters are the same used by Fanti et al. (2016).

Table 1: Parameters used to define the scroll walls geometry

Parameter	Symbol	Value
Nominal orbiting radius	r_o	6.5 mm
Radius of the involute basic circle	r_b	$23/2\pi$ mm
Wall thickness	e	5 mm
Initial angle of external involute	φ_{e0}	$-e/2r_b$
Initial angle of internal involute	φ_{i0}	$e/2r_b$
External starting angle	φ_{es}	$\pi/2$
Internal starting angle	φ_{is}	$\pi/2$
Involute final angle	φ_{max}	$15\pi/2$

The optimum pressure ratio for the scroll expander, the condition that should result in maximum isentropic efficiency, is defined by Eq. (9).

$$rp_{optimum} = rv^k \tag{9}$$

where *rv* is the volume ratio and *rp* is the pressure ratio between inlet and outlet of the expander. The ratio of specific heats *k* can be considered constant for the temperature range observed in the simulations.

The scroll expander prototype used for validation (Fanti et al., 2016) has volume ratio equal to 3, which results in optimum pressure ratio 4.65. Under-expansion or over-expansion would appear when pressure ratio differs from this value. However, experiments conducted by Romão (2017) presented maximum efficiency at a significant lower pressure ratio value.

3. NUMERICAL MODEL

3.1 Flow model

We used the numerical code Ansys CFX version 17 for conducting the CFD simulations. Ansys CFX solves conservation equations for mass, momentum and energy in a conservative form to characterize the flow.

Ideal gas model was used to characterize air properties. The transient and compressible flow in the expander was considered, without heat transfer in the walls. A fixed value was used for the air specific heat at constant pressure, considering the ambient temperature. The high order scheme was used to discretize the convection terms and the transient term were discretized with the second-order backward Euler scheme.

The SST *k-ω* turbulence model was chosen. This model switches between the models Wilcox *k-ω* and the *k-ε*, presenting advantages of both (good performance near the wall and in fully turbulent regions).

3.2 Computational grid

A simulation of a scroll expander requires a moving mesh, that gets too deformed during the simulation. Thereby we create two domains: the scroll domain, where the mesh can be deformed and substituted (moving mesh) and the stationary domain where the mesh will be fixed, see Fig. 1. With this division the meshes are generated separately for each computational domain, making possible to substitute only the mesh that is moving. The remesh is characterized by the interpolation of the results obtained with a current deformed mesh to a new one.

The inlet is located in the innermost part of the stationary scroll, while the outlet is located on the external circumference of the stationary domain, as showed in Fig. 1. A quasi-2D structured hexahedral mesh was employed on these simulations to save computational time, totalizing 50036 elements.

Monitoring some parameter that evaluates the grid quality is necessary to know when make the remesh procedure. In this work we monitor the orthogonality angle as described in Silva et al. (2016). We create a function that increases the periodicity of the remesh procedure when the orbiting angle gets close to 180 degrees. It is necessary because central extremity of mobile scroll approximates too much of the fix scroll wall (see Fig. 2), where the mesh loses quality abruptly by the movement of the orbiting scroll (the center is the region where the grid is more affected by the scroll movement) .This approach changes the grid 39 times in each revolution.

Since the grid substitution procedure occurs at the same angle values, for successive revolutions, it is possible to generate all mesh files before the simulation starts. Although this methodology takes more time on pre-processing, it results in a significantly more efficient simulation: the mesh substitution is performed based on an interrupt condition that only selects the proper mesh previously created, instead of generating it. We should emphasize that the simulation takes more than one revolution to finish and mesh substitution occurs at the same orbiting angles for different revolutions.

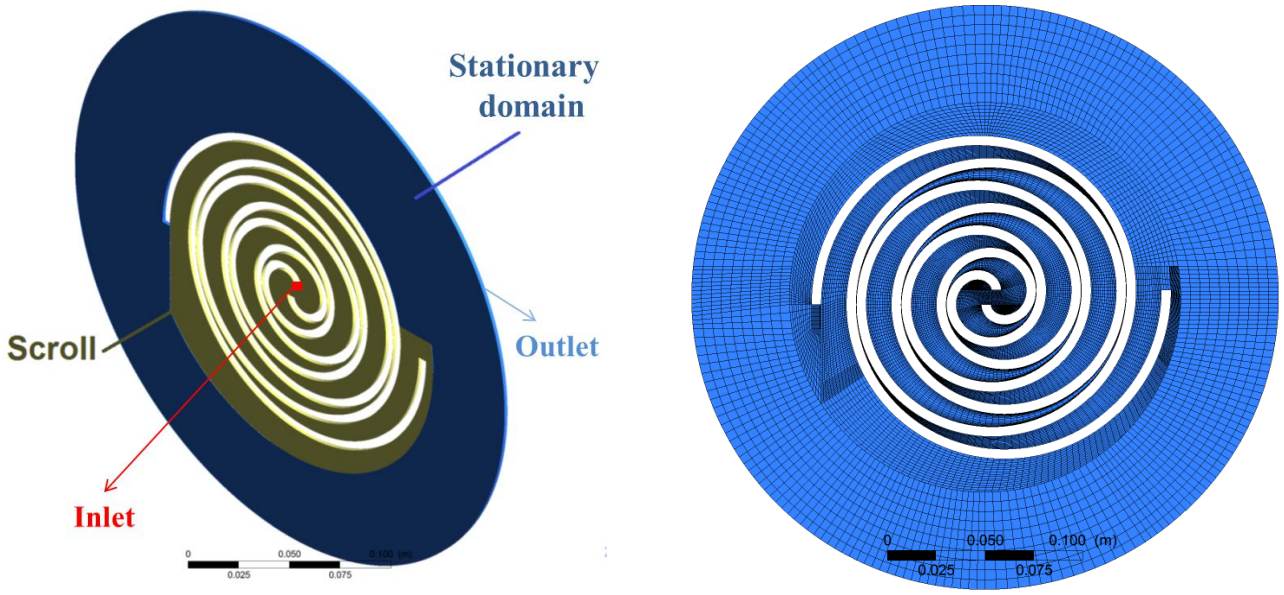

Figure 1: Domains and structured mesh used on CFD simulations

The advantages of the structured mesh are evident: Silva et al. (2016) on their CFD simulation required 116 remesh procedures using an unstructured mesh, besides being hard to guarantee sufficient mesh resolution in flank gaps. In addition, the structured grid ensures that during all the simulation the orthogonality angle is higher than 10°, what helps reducing numerical errors.

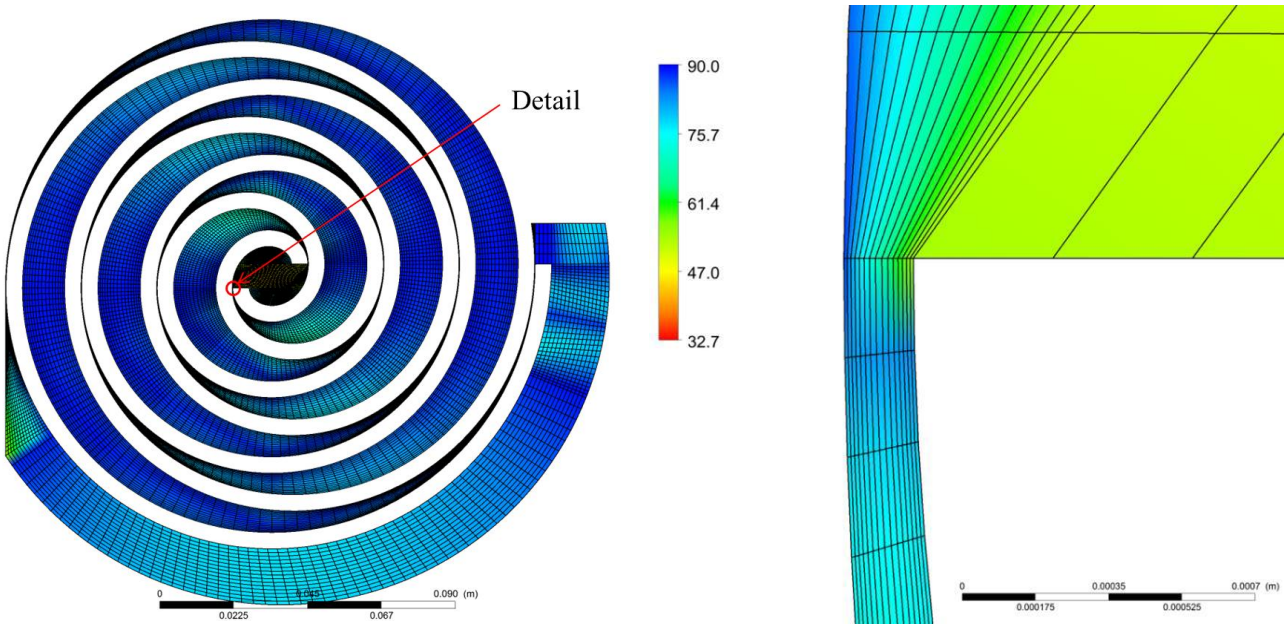

Figure 2: Mesh detail for an orbit angle of 179 degrees

3.3 Boundary conditions

Total pressure and total temperature was imposed at the scroll inlet, pressure and temperature (atmospheric conditions) were imposed in the outlet. An opening boundary condition was used in the expander outlet, where the fluid can get in or get out the fluid domain (stationary domain), as a far field condition. Inlet total pressure was variated to evaluate the influence of the pressure ratio on the results. The rotational speed was constant equal to the experimental tests available for comparison. These values of pressure, temperature and rotation correspond to experimental tests of Romão (2017), with the scroll prototype expanding air. Table 2 summarizes the boundary conditions used on the CFD simulations.

Table 2: Boundary conditions used on the CFD simulations

Parameter	Value
Inlet total pressure	1.5 to 4.7 bar
Atmospheric pressure	0.92 bar
Pressure ratio	1.6 to 5.1
Inlet total temperature	20°C
Outlet total temperature	20°C
Angular displacement per time step	0.2°
Rotational speed	2600 rpm

The convergence criteria used for the solution of mass, momentum and energy equations was RMS of normalized residuals lower than 10^{-4}. Courant number was monitored in order to grant numerical accuracy in the transient simulations performed.

In order to guarantee a stable behavior, the simulation ran for 4 revolutions of the scroll. In the first revolution the pressures increases linearly to avoid divergence, and is maintained constant after that. Silva et al. (2016) analyzing 10 complete revolutions of the scroll expander noted that, after the third revolution, there was repeatability of the results (two successive revolutions that present the same results).

3.4 Parameters to characterize the scroll performance

Two main parameters are used to characterize the scroll expander performance: isentropic efficiency and filling factor. These parameters were proposed by Zanelli and Fravat (1994) and have been used by others, sometimes with subtle differences. Isentropic efficiency and filling factor are given by Eq. (2) and Eq. (3), respectively:

$$\varepsilon = \frac{\dot{W}_{sh}}{\dot{m}\left(h_{su} - h_{ex,s}\right)} \tag{10}$$

$$\phi = \frac{\dot{m}\, v_{su}}{\dot{V}_{su}} \tag{11}$$

where $\dot{W}_{sh}$ is the shaft power, $\dot{m}$ is the mass flow rate, h_{su} is the specific enthalpy at inlet, $h_{ex,s}$ is the specific isentropic enthalpy at outlet, v_{su} is the specific volume at inlet and $\dot{V}_{su}$ is the volumetric displacement rate.

4. RESULTS AND DISCUSSIONS

The results obtained with the transient simulation for mass flow rate and shaft power are presented in Fig. 3, considering the period of one complete revolution. The revolution considered to obtain these results is the last one, in order to guarantee stability. Average mass flow rate and power may be obtained from instantaneous values presented in Fig.3.

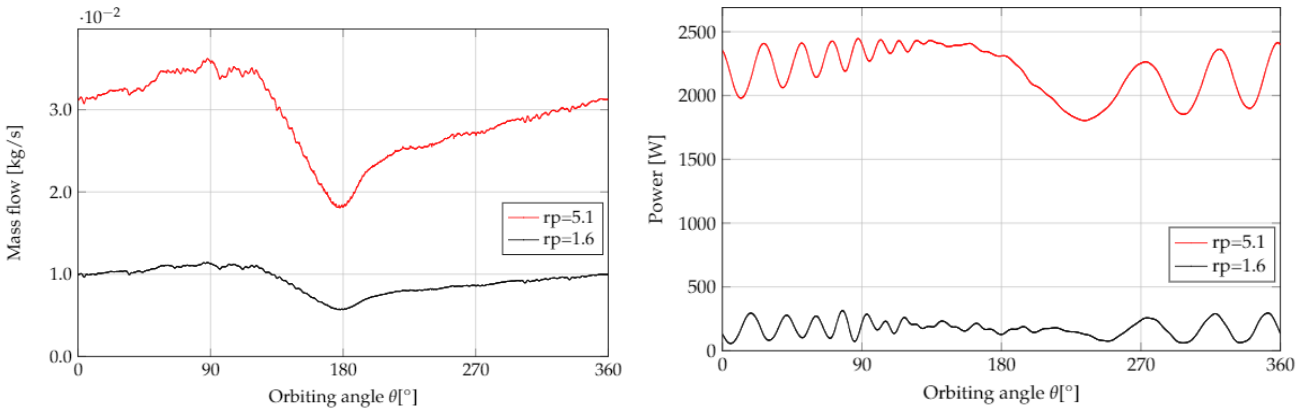

Figure 3: Instantaneous mass flow rate and power during one revolution after stabilization.

The filling factor relates the measured mass flow rate and the theoretical mass flow rate. It is important to point out that the internal leakages can result in a filling factor higher than one. Besides, there is a possibility that this factor is less than one, due the pressure drop at inlet. This last condition commonly occurs at high rotational speed range.

Figure 4 shows the behavior of the filling factor during one revolution for two values of pressure ratio simulated, resulting in no significant difference between the two curves. Therefore, the filling factor practically remains constant with the pressure ratio variation. Romão (2017) observed similar results in his experimental analysis, which considered the same range of pressure ratio variation.

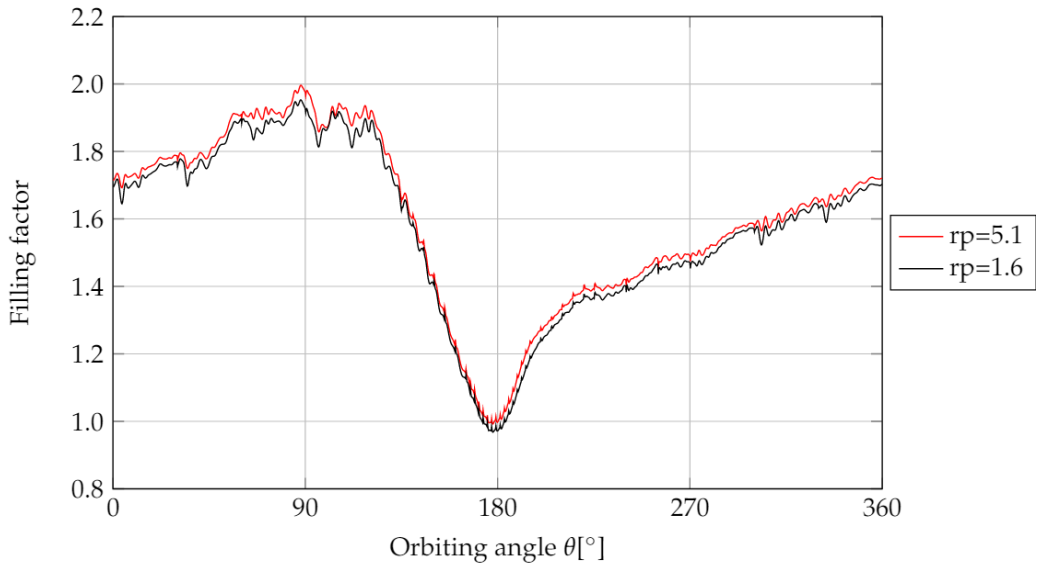

Figure 4: Filling factor variation during a revolution for two different values of pressure ratio.

Figures 5 to 8 show the results obtained numerically with CFD simulations compared to experimental results obtained by Romão (2017). The mass flow rate as a function of pressure ratio is shown in Fig. 5 when rotation is maintained constant at 2600 rpm. Clearly, the simulation presents lower mass flow rate prediction when compared to experiments. The reason for this difference can be attributed to inaccuracy in the characterization of internal leakages. The scroll prototype tested by Romão (2017) present the same flank gap between the walls of fixed and moving scroll walls that we used in present work. However, due to the geometry of the sealing used in the top of prototype scroll parts the actual leakage cross-sectional area is 44% higher in the prototype than in the geometry used for CFD simulations. This area difference is responsible for the inaccuracy in mass flow rate prediction observed in Fig. 5.

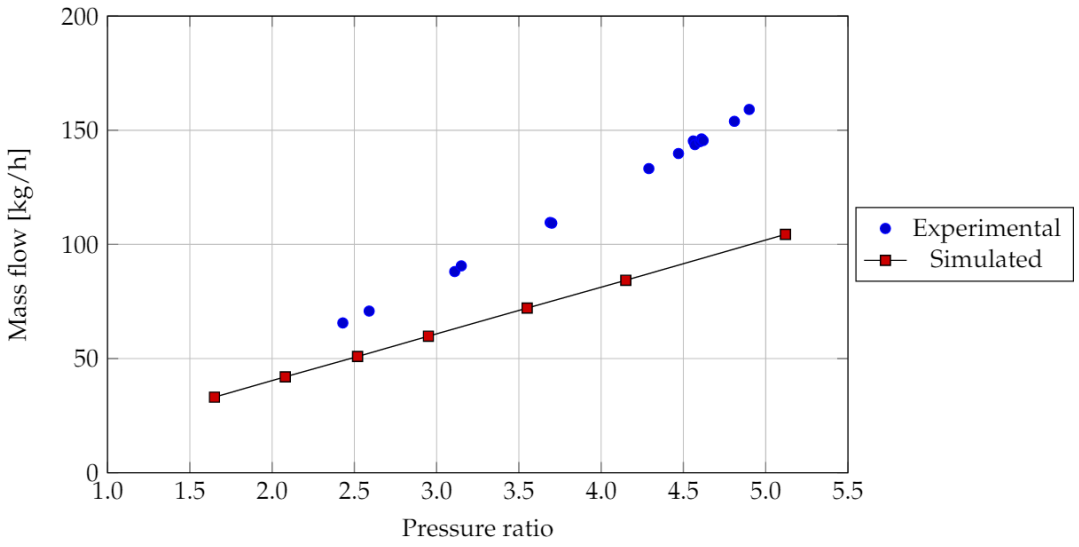

Figure 5: Mass flow rate as a function of pressure ratio: CFD simulation versus experiments by Romão (2017).

Similar comparison is presented for shaft power in Fig. 6. Shaft power presents the clear tendency of linear increase with pressure ratio. This is in agreement with experiments obtained by Romão (2017) and other similar results in literature. It is important to note that simulation results do not take into account internal friction present in rolling bearings and internal sealing and higher power prediction than experiments was expected. Due to this, the 17% differences observed in Fig. 6 may be considered very satisfactory.

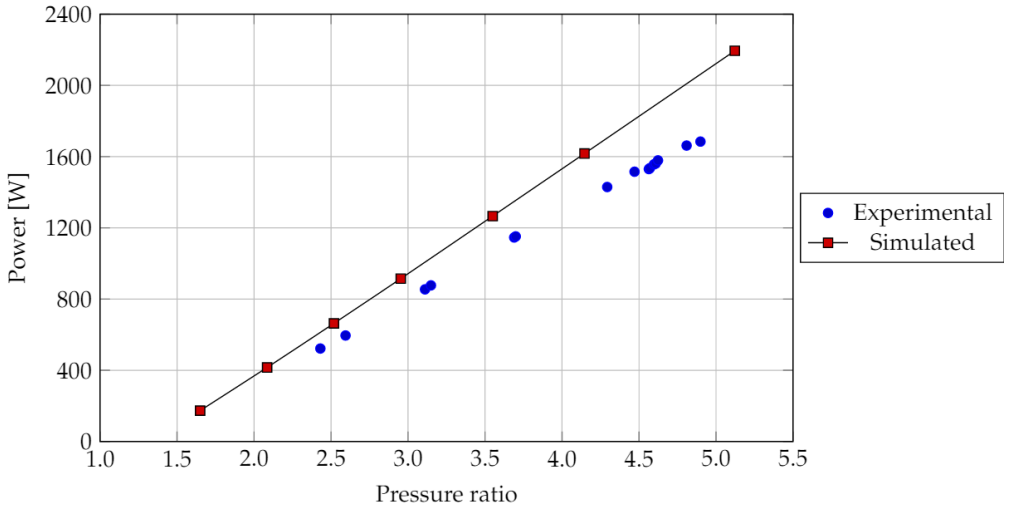

Figure 6: Power as a function of pressure ratio: CFD simulation versus experiments by Romão (2017).

Figure 7 presents the isentropic efficiency as a function of pressure ratio. The maximum efficiency in numerical results occurs for pressure ratio close to 3.5, corresponding to 70.7%, and is significantly different from the optimum value of 4.65 given by Eq. 9. The careful analysis of CFD results reveals that the flank clearance of the prototype (165 µm) is too high and causes intense internal leakages between the chambers, which result in an increased final pressure on the last scroll chamber. Therefore, under-expansion occurs when pressure ratio is 4.65, reducing isentropic efficiency.

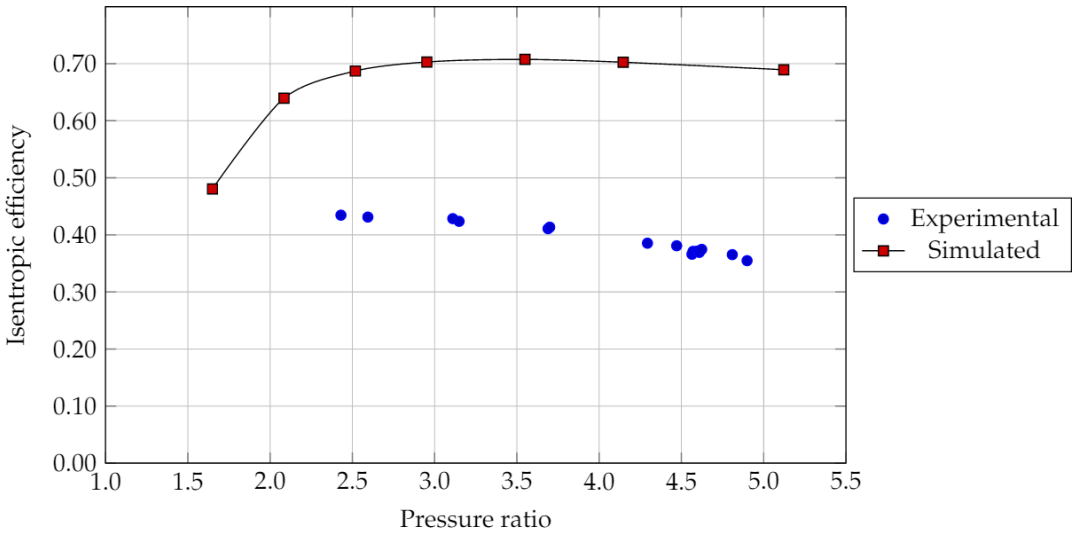

Figure 7: Isentropic efficiency as a function of pressure ratio: CFD simulation versus experiments by Romão (2017).

The high difference observed in CFD prediction of isentropic efficiency when compared to experiment (Figure 7) is related to inaccuracy in predicting mass flow rate, already presented and discussed in Fig. 5.

The CFD simulation considered internal leakages occurring only in the flank clearance (0.165 mm × 40 mm), but the geometry of the mechanical seals used in the prototype result in an increased leakage area (Fig.8). Actually, the leakage cross-sectional area is 44% higher in the prototype than in the geometry used for CFD simulations. It explains the differences verified in CFD predictions of mass flow rate and isentropic efficiency.

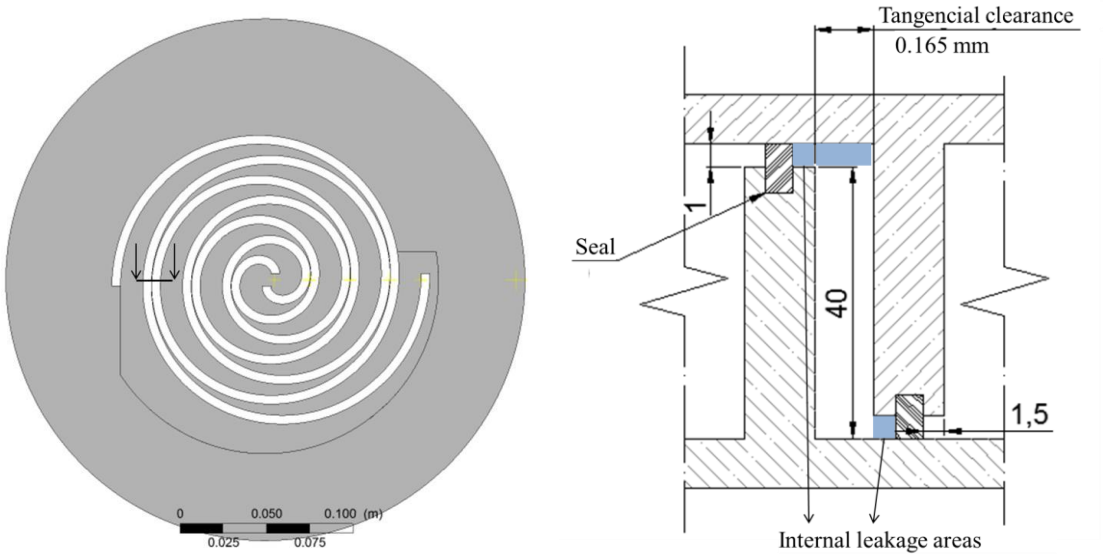

Figure 8: Flank clearance where internal leakages occur.

Figures 9 and 10 evidence the under-expansion and over-expansion events when the pressure ratio is significantly different than 3.5 (the point of maximum efficiency on numerical simulations). It explains the results obtained for the isentropic efficiency. The pressure at p1, p2 and p3 are computed at the three scroll chambers, going from innermost to outermost chamber, while ”p in” and “p out” are the inlet and outlet pressure.

Although in Fig. 9 the value of pressure ratio is smaller than 4.65 (optimum value) for which is expected an over-expansion, clearly there is an under-expansion. It permits to conclude that the optimum value for pressure ratio given by Eq. 9 is valid only in a condition without leakages.

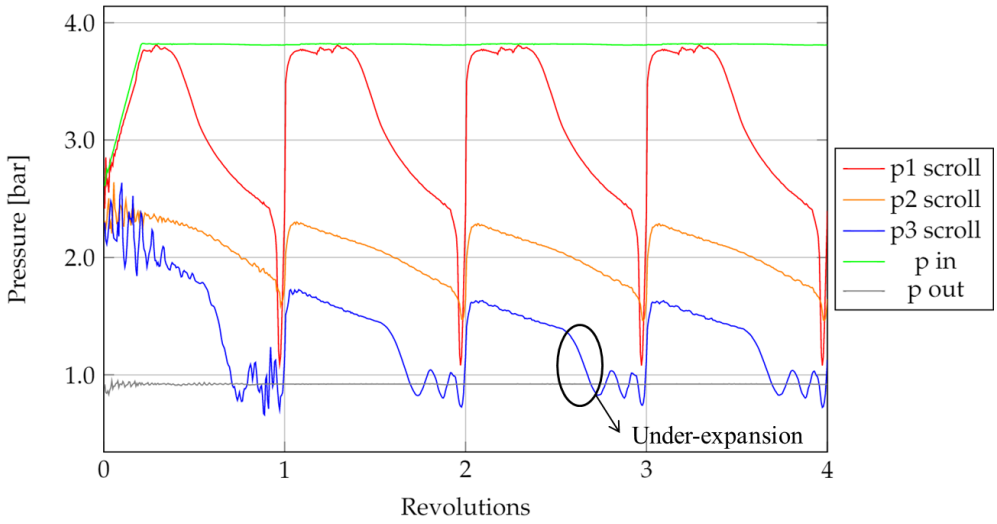

Figure 9: Under-expansion visualization for pressure ratio equal to 4.1.

Oscillations present between pressures of subsequent chambers in the Fig. 9 and 10 are due to shock waves. The flank leakages can be characterized as a leakage by a convergent-divergent nozzle, with the same minimum area. After pass through the throat and achieve Mach equal to 1, the flow continues to accelerate until it becomes inconsistent. So an abrupt variation on the properties occurs at the internal gaps, reducing the flow velocity to subsonic values and characterizing a shock wave.

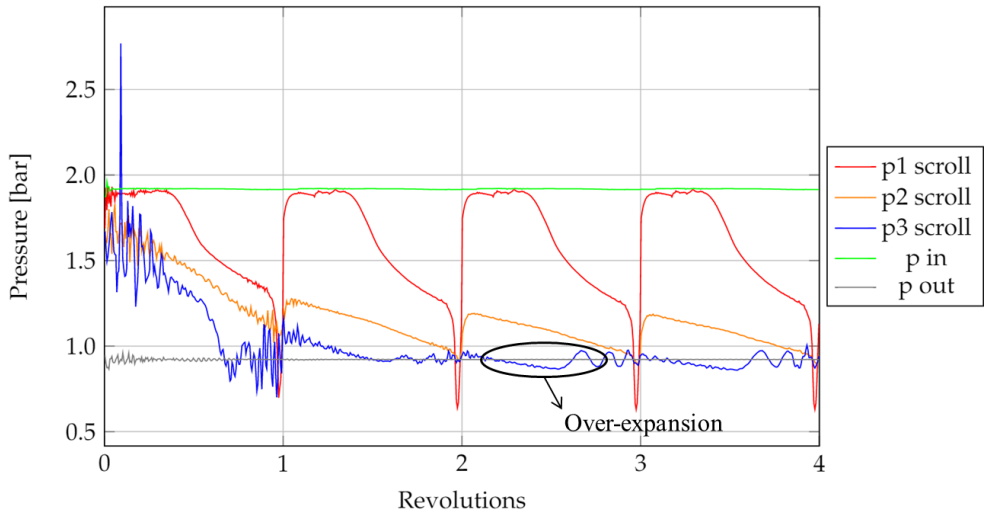

Figure 10: Over-expansion visualization for pressure ratio equal to 2.1.

The pressure and Mach distribution in the internal gaps are shown in Fig. 11. This effect influences the internal leakages that are occurring on the scroll and the filling factor. The proper characterization of the internal leakages is essential to obtain reasonable prediction for the scroll efficiency.

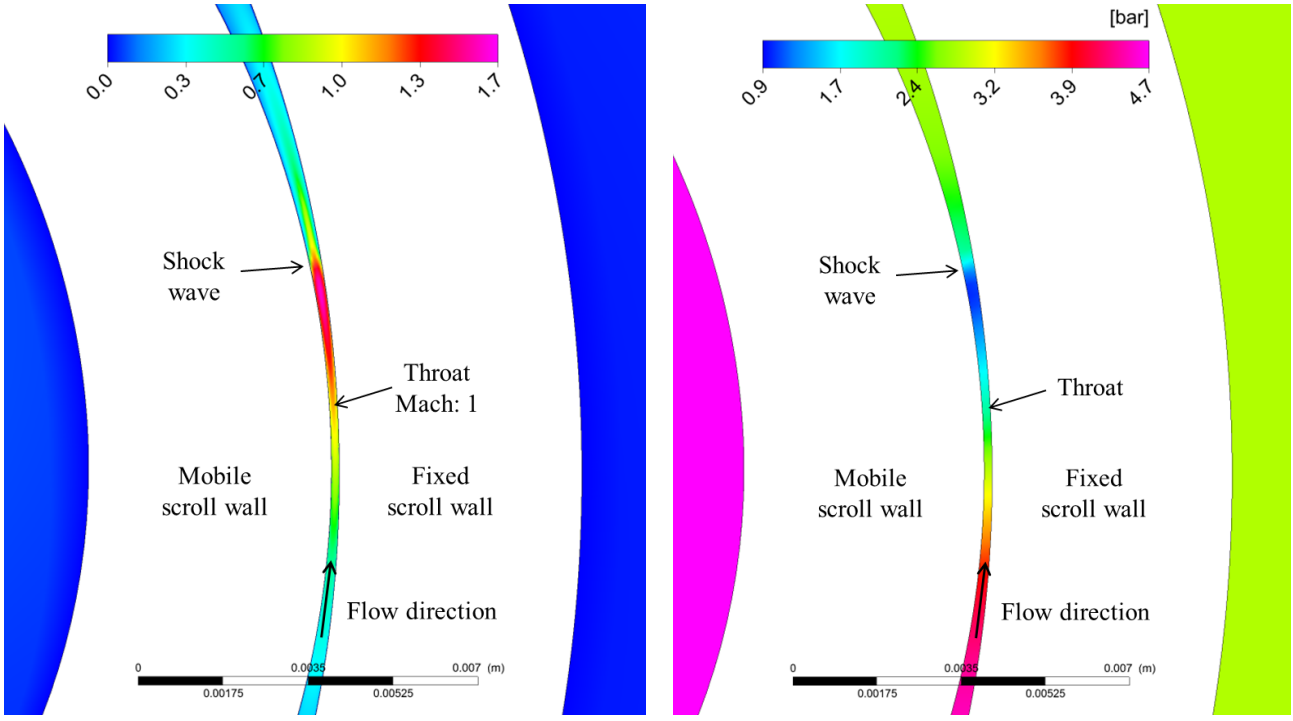

Figure 11: Mach number and pressure variation on the internal leakages.

5. CONCLUSIONS

For a constant rotation speed, filling factor remains almost constant, despite the pressure ratio variation. This behavior indicates that the internal leakages also are not influenced by pressure ratio, at least in the range investigated in present work. This result is in accordance with experimental observations by Romão (2017).

However, variations in pressure ratio cause over-expansion or under-expansion decreasing the isentropic efficiency of the scroll expander. The CFD simulations conducted were capable of predicting power with a minimum deviation if compared to experiments. This difference may be attributed to friction in the prototype, not characterized experimentally.

Internal clearances affect the value of pressure ratio where maximum isentropic efficiency occurs. The larger the clearances, the smaller will be the value of optimum pressure ratio.

Results presented in this paper were obtained with two dimensional simulations. In order to characterize pressure drop at inlet, three dimensional simulations are needed. Besides, heat transfer in the external walls was not included in the simulation yet.

6. ACNOWLEDGEMENTS

The authors would like to acknowledge Centro Universitário da FEI and Fundação de Amparo à Pesquisa do Estado de São Paulo (FAPESP, Process No. 2011/17657-7) for the research support.

7. REFERENCES

Blunier, B., Cirrincione, G., Hervé, Y., & Miraoui, A. (2009). A new analytical and dynamical model of a scroll compressor with experimental validation. International journal of refrigeration, 32(5), 874-891.

Declaye, S., Quoilin, S., Guillaume, L., & Lemort, V. (2013). Experimental study on an open-drive scroll expander integrated into an ORC (Organic Rankine Cycle) system with R245fa as working fluid. Energy, 55, 173-183.

Fanti, G. R., Donato, G.H.B., De Mello, P. E. B., (2016). A novel scroll expander for flank leakage investigation: preliminary tests. In: 29th International Conference on Efficiency, Cost, Optimisation, Simulation and Environmental Impact of Energy Systems, Portoroz. Ljubljana, 2016.

Mendoza, L. C., Navarro-Esbrí, J., Bruno, J. C., Lemort, V., & Coronas, A. (2014). Characterization and modeling of a scroll expander with air and ammonia as working fluid. Applied Thermal Engineering, 70(1), 630-640.

Quoilin, S., Van Den Broek, M., Declaye, S., Dewallef, P., & Lemort, V. (2013). Techno-economic survey of Organic Rankine Cycle (ORC) systems. Renewable and Sustainable Energy Reviews, 22, 168-186.

Romão, D. A. (2017). Experimental analysis of internal leakage effects over the performance of scroll expanders, Master´s Dissertation, in Portuguese.

Silva, F. M. F., Oliveira, F. V., De Mello, P. E. B., (2016). Simulation strategy of a novel scroll expander using remesh technique. In: 16th Brazilian Congress of Thermal Sciences and Engineering, Vitória. Brazil, 2016.

Silva, F. M. F. (2017). Strategy for CFD simulations of a scroll expander, Master´s Dissertation, in Portuguese.

Song, P., Wei, M., Shi, L., Danish, S. N., & Ma, C. (2015a). A review of scroll expanders for organic Rankine cycle systems. Applied Thermal Engineering, 75, 54-64.

Song, P., Wei, M., Liu, Z., & Zhao, B. (2015b). Effects of suction port arrangements on a scroll expander for a small scale ORC system based on CFD approach. Applied Energy, 150, 274-285.

Wei, M., Song, P., Zhao, B., Shi, L., Wang, Z., & Ma, C. (2015). Unsteady flow in the suction process of a scroll expander for an ORC waste heat recovery system. Applied Thermal Engineering, 78, 460-470.

Yanagisawa, T., Fukuta, M., Ogi, Y., & Hikichi, T. (2001). Performance of an oil-free scroll-type air expander. In Proc. of the ImechE Conf. Trans. on compressors and their systems (No. C591/027, pp. 167-174).

Zanelli, R., Favrat, D. (1994). Experimental investigation of a hermetic scroll expander-generator. In: International Compressor Engineering Conference. Paper 1021.

8. RESPONSIBILITY NOTICE

The authors are the only responsible for the printed material included in this paper.